Rapid and stable collective charging and discharge suppression in many-body quantum batteries

Yi-Fan Yang(杨伊凡), Shun-Cai Zhao(赵顺才)

Citation: Chin. Phys. B. 35, 104206 (2026). DOI: 10.1088/1674-1056/ae3b31 | CSTR: 32038.14.CPB.ae3b31
http://cpb.iphy.ac.cn; http://iopscience.iop.org/cpb

What follows is a list of articles you may be interested in

Enhancement of electromagnetically induced absorption and four-wave mixing in a double two-level system

Yu-Sen Wang(王禹森), Ying-Jie Du(杜英杰)
Chin. Phys. B. 34, 124201 (2025). DOI: 10.1088/1674-1056/ade8e1 | CSTR: 32038.14.CPB.ade8e1

Rapid hologram generation through backward ray tracing and adaptive-resolution wavefront recording plane

Jianying Zhu(朱建英), Yong Bi(毕勇), Minyuan Sun(孙敏远), Weinan Gao(高伟男)
Chin. Phys. B. 33, 114204 (2024). DOI: 10.1088/1674-1056/ad7c2e

Effect of the target positions on the rapid identification of aluminum alloys by using filament-induced breakdown spectroscopy combined with machine learning

Xiaoguang Li(李晓光), Xuetong Lu(陆雪童), Yong Zhang(张勇), Shaozhong Song(宋少忠), Zuoqiang Hao(郝作强), Xun Gao(高勋)
Chin. Phys. B. 31, 054212 (2022). DOI: 10.1088/1674-1056/ac3810

Simple and robust method for rapid cooling of ^{87}Rb to quantum degeneracy

Chun-Hua Wei(魏春华), Shu-Hua Yan(颜树华)
Chin. Phys. B. 29, 064208 (2020). DOI: 10.1088/1674-1056/ab8625

Optical modulation of repaired damage site on fused silica produced by CO_2 laser rapid ablation mitigation

Chao Tan(谭超), Lin-Jie Zhao(赵林杰), Ming-Jun Chen(陈明君), Jian Cheng(程健), Zhao-Yang Yin(尹朝阳), Qi Liu(刘启), Hao Yang(杨浩), Wei Liao(廖威)
Chin. Phys. B. 29, 054209 (2020). DOI: 10.1088/1674-1056/ab8206

Rapid and stable collective charging and discharge suppression in many-body quantum batteries

Yi-Fan Yang(杨伊凡) and Shun-Cai Zhao(赵顺才)†

Center for Quantum Materials and Computational Condensed Matter Physics, Faculty of Science, Kunming University of Science and Technology, Kunming 650500, *China*

(Received 21 November 2025; revised manuscript received 18 January 2026; accepted manuscript online 21 January 2026)

Achieving rapid and stable energy storage in quantum batteries (QBs) remains a key challenge, particularly under strong system–environment coupling where non-Markovian effects become prominent. While most previous studies focus on weak coupling regimes, we propose a many-body QB model exhibiting collective charging and discharge suppression in a non-perturbative regime. The model adopts a Λ-type configuration where multiple battery units share a common excited state and have individual ground states, forming an effective collective structure. To accurately capture the dynamics under strong coupling, the system's time evolution is governed by a Redfield-type master equation incorporating memory effects via a Debye spectral density. We quantify the stored energy using ergotropy and analyze the impact of tunneling, driving strength, spectral width, and environmental temperature on charging performance. Numerical simulations reveal that optimized driving and reservoir engineering can simultaneously achieve rapid and stable charging while suppressing energy leakage. These results provide theoretical insights into strong-coupling thermodynamics and guide the design of robust QB platforms using solid-state or atomic systems.

Keywords: many-body quantum battery, ergotropy dynamics, rapid-stable charging, strong coupling, non-Markovian dynamics

PACS: 42.50.Gy, 03.65.Yz, 05.70.Ln

DOI: 10.1088/1674-1056/ae3b31 **CSTR:** 32038.14.CPB.ae3b31

1. Introduction

Quantum batteries (QBs), envisioned as atomic-scale energy storage and conversion devices, have emerged as a promising component in quantum technologies.[1,2] The miniaturization of quantum devices[3] has motivated fundamental investigations into whether quantum coherence and correlations can be exploited to enhance charging efficiency.[4,5] Two principal charging paradigms have been proposed: the *parallel charging* scheme, where each quantum cell is charged independently,[5] and the *collective charging* scheme, where a global unitary drives the entire system coherently.[6,7] Recent efforts have revealed that collective protocols can yield a quantum advantage in both charging speed and power.[8–11]

In addition to charging performance, researchers have explored energy extraction from QBs in realistic noisy environments. Tirone *et al.*[12] showed that nonlocal correlations can mitigate noise-induced degradation during work extraction. Similarly, remote charging schemes.[13] and coherent collision models.[14] have been introduced to suppress energy loss and improve the robustness of quantum batteries. In particular, the role of quantum coherence in enabling faster charging and higher ergotropy has been highlighted.[15]

Despite these advances, most previous studies assumed weak system–environment coupling and Markovian dynamics.[16–18] However, in practical implementations — such as quantum dots, superconducting circuits, or Rydberg atom arrays — quantum systems often interact strongly with their environments, resulting in non-Markovian dynamics. The validity of conventional Lindblad or Born–Markov master equations becomes questionable in such regimes.[19,20] Thus, a key open question is: can collective effects still offer performance advantages under strong coupling and memory effects? And if so, how can energy leakage or reverse flows be effectively suppressed?

In this work, we propose a strongly coupled many-body QB model operating in a non-perturbative regime. The model adopts a Λ-type collective configuration (as schematically shown in Fig. 1(b)), in which multiple QBs share a common excited state $|e\rangle$ while maintaining distinct ground states $|g_i\rangle$. This structure is effectively equivalent to an N-level system with a single excited state, enabling collective dynamics. The system's dynamics are governed by a Redfield-type master equation incorporating non-Markovian effects through spectral engineering. We quantify the stored energy and extractable work (ergotropy) and systematically analyze how various physical parameters — such as driving strength, energy gap, tunneling interaction, and environment temperature — affect the charging performance.

The rest of this paper is organized as follows: In Sec-

†Corresponding author. E-mail: zsczhao@126.com

© 2026 Chinese Physical Society and IOP Publishing Ltd. All rights, including for text and data mining, AI training, and similar technologies, are reserved.

tion 2, we construct a many-body collective QB model with an effective two-level structure. In Section 3, the energy storage and work extraction dynamics are formulated based on ergotropy. In Section 4, to balance computational cost and analytical clarity, we analyze a three-qubit QB example to study rapid-stable charging and discharging suppression. Finally, we summarize our findings in Section 6.

2. Many-body collective QB model

To explore QB behavior beyond weak coupling, we consider a one-dimensional many-body QB system strongly coupled to a bosonic environment. As illustrated in Fig. 1(a), each unit cell (battery) features a similar excited state $|1\rangle$ (representing the fully charged state) and an individual ground state $|i\rangle$ $(i=2,\ldots,n)$ (corresponding to fully discharged configurations), where each battery can independently perform external charging in a parallel configuration. In Fig. 1(b), by contrast, the discharged states $|i\rangle$ of adjacent battery units are interconnected through tunneling interactions (uniformly characterized by a constant coupling parameter T_e), forming an effective Λ-type structure that creates quantum interference effects in charge transport and enables a collective charging mechanism. Such configurations can be physically realized in multilevel quantum dot arrays,[21] engineered spin-1 systems[22] or Rydberg atom platforms.[23] Even when idealized, this structure captures essential features of coherence-enhanced storage and collective dynamics, and is widely used in quantum optics for modeling effects such as dark-state superpositions and electromagnetically induced transparency (EIT).[24] For both configurations, we denote the time-dependent charging field applied to each battery unit by $\Omega_i(t)$ for $i=2,3,\ldots,n-1$, and the system–environment coupling strength for each unit is described by $g_i(\omega_i)$. This abstraction captures the essence of both parallel and collective charging dynamics — where units either function independently or interact coherently through shared degrees of freedom.

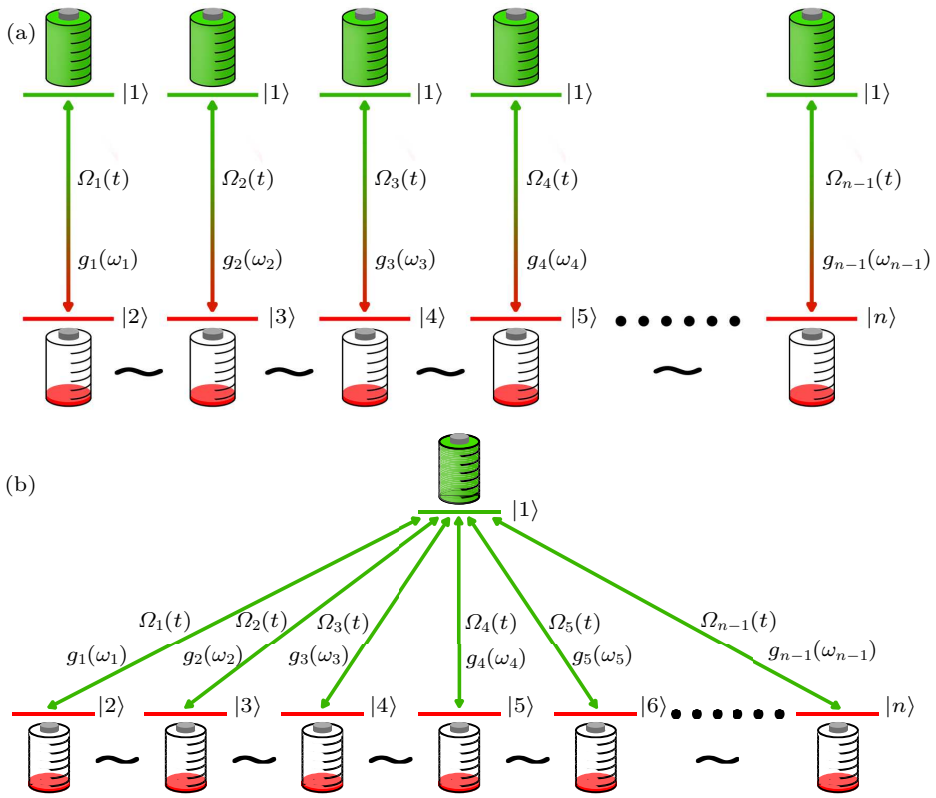

Fig. 1. Schematic illustration of two charging schemes for many-body quantum batteries. (a) Parallel charging scheme: Multiple independent two-level systems (qubits), each with its own ground $|i\rangle$ and excited $|1\rangle$ states, are charged simultaneously by individual fields $\Omega_i(t)$. (b) Collective charging scheme (studied in this work): An effective Λ-type system where all battery units share a single common excited state $|1\rangle$ and possess individual ground states $|i\rangle$. The system is charged by a global driving field that couples the ground states to the common excited state. The wavy lines represent possible tunneling between ground states.

The total Hamiltonian is given by

$$\hat{H}=\hat{H}_{\rm S}+\hat{H}_{\rm E}+\hat{H}_{\rm int}, \tag{1}$$

where $\hat{H}_{\rm S}$ describes the QB system, $\hat{H}_{\rm E}$ the environment, and $\hat{H}_{\rm int}$ the interaction between them.

The system Hamiltonian incorporates time-dependent driving and tunneling between neighboring battery units:

$$\hat{H}_{\rm S}=\varepsilon_1\hat{\sigma}_1+\sum_{j=2}^{n}\Omega_j(t)|1\rangle\langle j|+\sum_{j=2}^{n-1}T_{\rm e}|j\rangle\langle j+1|+{\rm H.c.}, \tag{2}$$

where $\Omega_j(t)$ denotes the external driving field that governs the charging process as shown in Fig. 1(b). The driving func-

tion $\Omega_j(t)$ is typically sinusoidal or periodic to mimic realistic modulation. In Eq. (2), the parameter T_e denotes the quantum tunneling amplitude between adjacent ground states $|j\rangle$ and $|j+1\rangle$. This tunneling effect effectively induces a coherent coupling (or interaction) between the corresponding battery units, facilitating the transfer of excitations and the establishment of many-body correlations across the QB array. ε_i are the level energies.

The environment is modeled as a bath of harmonic oscillators, consistent with the Debye model:[25]

$$\hat{H}_{\mathrm{E}} = \sum_k \omega_k \hat{a}_k^{\dagger} \hat{a}_k, \tag{3}$$

with cutoff frequency ω_{D}, typically satisfying $\omega_k \leq \omega_{\mathrm{D}}$. In our numerical calculations for the collective Λ-type model, the system–environment interaction is specifically chosen to describe dephasing noise on the ground-state manifold. The interaction Hamiltonian is given by

$$\hat{H}_{\mathrm{int}} = \sum_{i=2}^{n} \sum_k g_k^{(i)} \hat{A}_{\mathrm{S}}^{(i)} \otimes \hat{B}_k, \tag{4}$$

where the system operator $\hat{A}_{\mathrm{S}}^{(i)} = |g_i\rangle\langle g_i|$ is the projector onto the i-th ground state, and the bath operator $\hat{B}_k = (\hat{a}_k^{\dagger} + \hat{a}_k)$ is the position quadrature of the k-th bath mode. This coupling leads to energy-conserving dephasing, which disrupts the phase coherence between the ground states and the common excited state, a primary mechanism of ergotropy loss in our system.

To highlight the collective effects studied here, it is instructive to contrast our model with a parallel charging scheme. In a parallel scheme of N true qubits (shown in Fig. 1(a)), the system Hamiltonian would be

$$\hat{H}_{\mathrm{S}}^{\mathrm{parallel}} = \sum_{i=1}^{N} \varepsilon_i \hat{\sigma}_i + \sum_{j=2}^{N} \Omega_j(t) |1\rangle\langle j| + \mathrm{H.c.}, \tag{5}$$

where the key difference lies in the structure of the excited states: the parallel scheme has N excitable degrees of freedom and lacks quantum interference effects between adjacent battery units, whereas our collective Λ-model (shown in Fig. 1(b)) has only one and exhibits quantum interference between adjacent battery units, leading to fundamentally different collective dynamics and robustness, as demonstrated in our numerical results. Here, $|1\rangle$ denotes the common excited state shared by all battery units in the Λ-type collective structure, hence no unit-specific subscript is required.

To capture open-system dynamics under strong coupling, we adopt a Redfield-type master equation[26–29] (see Appendix A for details):

$$\begin{aligned} \frac{\mathrm{d}}{\mathrm{d}t}\hat{\rho}(t) \;=\; & -\frac{\mathrm{i}}{\hbar}\left[\hat{H}_{\mathrm{S}}(t), \hat{\rho}(t)\right] \\ & + \sum_{i,j} R_{ij}\left(2\hat{L}_{ij}\hat{\rho}(t)\hat{L}_{ij}^{\dagger} - \{\hat{L}_{ij}^{\dagger}\hat{L}_{ij}, \hat{\rho}(t)\}\right), \end{aligned} \tag{6}$$

where $\hat{L}_{ij} = |i\rangle\langle j|$ denotes Lindblad-like jump operators, and $R_{ij}(\omega)$ is the Redfield tensor element that characterizes dissipative transitions between states. In contrast to Markovian Lindblad forms, the Redfield tensor explicitly depends on both the environmental spectral density and temperature.

In the Redfield master Eq. (6), the jump operators $\hat{L}_{ij} = |i\rangle\langle j|$ connect the eigenstates of the system Hamiltonian $\hat{H}_{\mathrm{S}}$. The specific form of the Redfield tensor $R_{ij}(\omega)$ is derived from the spectral density of the bath and the matrix elements of the system coupling operator $\hat{A}_{\mathrm{S}}$ defined above (Eq. (4)), projected onto the system's energy eigenbasis.

$$R_{ij}(\omega) = J_{ij}(\omega)\left[\coth\left(\frac{\hbar\omega}{2k_{\mathrm{B}}T}\right) + 1\right], \tag{7}$$

where $J_{ij}(\omega)$ is the spectral density describing the coupling between the system and the environment. In this work, we consider a Debye-type form

$$J_{ij}(\omega) = \gamma_{ij}\frac{\omega}{\omega_0^2 + \omega^2}, \tag{8}$$

which captures the frequency-dependent interaction strength between the system and its environment, and reflects the finite memory (correlation) time of the bath. Spectral density functions such as the Debye,[30] Ohmic,[31] and Drude–Lorentz[32] models are widely employed in modeling different types of system–bath couplings in quantum open systems. The specific form of $J_{ij}(\omega)$ directly determines the structure of the Redfield tensor and thereby governs the dissipative dynamics of the system.

To illustrate this effect, Fig. 2 shows the behavior of the Redfield tensor $R_{ij}(\omega)$ at room temperature, evaluated using the Debye spectral density. As depicted, $J_{ij}(\omega)$ remains finite over the relevant frequency range, and both the environmental frequency ω_k and the spectral profile contribute to a suppression of the dissipative coefficients. This demonstrates how environmental structure modulates the decoherence and energy relaxation in the quantum battery system.

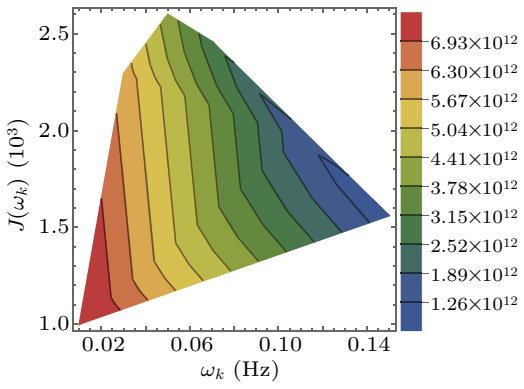

Fig. 2. Redfield tensor vs. the environmental frequency ω_k and Debye environmental spectral density $J(\omega_k)$ with other parameters being $\gamma = 2.6 \times 10^{-4}$ Hz, $T = 300$ K, $\omega_0 = 0.05$ Hz.

The Redfield master equation, though perturbative, offers a flexible framework for incorporating finite bath correlation times and capturing partial non-Markovian memory effects. Its applicability extends beyond the strict weak-coupling limit, particularly in structured or frequency-selective environments where the Born–Markov approximation fails. Recent studies have demonstrated its reliability in such contexts,[27,28] supporting its use here as a balance between analytical tractability and physical realism. In this work, we restrict our analysis to regimes where the Redfield approach remains quantitatively valid. Although it does not capture all non-perturbative features of the ultra-strong-coupling limit, it has been effectively applied to intermediate coupling and structured spectral densities.[27,29] The validity is determined by the dimensionless ratio of the system–bath coupling rate to the characteristic system frequency, which in our simulations lies within the moderate-coupling regime. Under these conditions, the Redfield equation provides a physically consistent and computationally efficient description of non-Markovian dynamics, retaining essential memory effects without the high cost of fully non-perturbative methods such as the hierarchical equations of motion (HEOM).

In the numerical implementation, the Redfield equation is integrated using a time-discretized scheme. To preserve the physical consistency of the density matrix $\hat{\rho}(t)$ — its trace and positivity — we apply a stabilization procedure at each time step: trace conservation is enforced by renormalization, and a positivity correction algorithm[33] is used when small negative eigenvalues occur. This ensures robust dynamics within the moderate-coupling regime considered. The physical validity of the results is further verified by confirming that, in the limits of weak driving and negligible coupling, the model reproduces coherent oscillations. Convergence with respect to time-step discretization has also been confirmed to ensure numerical stability.

3. Energy quantification

To evaluate QB performance we monitor both internal energy and dissipative losses. In regimes of strong system–environment coupling, non-Markovian memory effects render standard Born–Markov treatments inadequate. Accordingly, we employ a Redfield-type quantum master equation (Eq. (6)) with structured spectral densities to incorporate frequency-dependent dissipation; this choice is supported by recent studies targeting intermediate-to-strong coupling.[27,28] The performance of the QB is quantified by two key observables: internal energy and ergotropy, as follows.

Internal energy The energy stored in the QB at time t is given by

$$E(t) = \mathrm{Tr}\big[\hat{H}_{\mathrm{S}}\hat{\rho}(t)\big] - \mathrm{Tr}\big[\hat{H}_{\mathrm{S}}\hat{\rho}(0)\big], \tag{9}$$

which measures the net energy gained relative to the initial state.

Ergotropy To evaluate the extractable work under unitary operations, we employ the notion of ergotropy, defined as the energy difference between the system's instantaneous state and its passive counterpart:[34]

$$\mathcal{E}(t) = \mathrm{Tr}\big[\hat{H}_{\mathrm{S}}\hat{\rho}(t)\big] - \mathrm{Tr}\big[\hat{H}_{\mathrm{S}}\hat{\rho}_{\mathrm{pass}}(t)\big], \tag{10}$$

where the passive state $\hat{\rho}_{\mathrm{pass}}(t)$ associated with the density matrix $\hat{\rho}(t)$ in Eq. (10) is defined as the state that minimizes the energy under all possible cyclic unitary transformations U, such that $\hat{\rho}_{\mathrm{pass}} = \mathrm{argmin}_U \mathrm{Tr}[\hat{H}\hat{U}\hat{\rho}\hat{U}^{\dagger}]$. Following the seminal work by Allahverdyan *et al.*,[34] a state is passive if and only if it commutes with the system Hamiltonian $\hat{H}$ and its eigenvalues $\{r_j\}$ are arranged in a non-increasing order relative to the increasing energy eigenvalues $\{\varepsilon_j\}$ (i.e., $r_i \geq r_j$ if $\varepsilon_i < \varepsilon_j$). This configuration represents a state from which no ergotropy can be further extracted, serving as the fundamental reference point for quantifying the maximum extractable work in the quantum battery.

Before proceeding to numerical analysis, we illustrate the model behavior through a minimal collective configuration. A three-qubit example is introduced to explicitly examine the dynamical features of rapid charging and energy dissipation regulation under various parameter regimes. In the next section, we will numerically analyze the time evolution of the internal energy $E(t)$ and ergotropy $\mathcal{E}(t)$ under varying control parameters, including tunneling strength T_{e}, spectral cutoff ω_0, and driving amplitude V.

Having defined the energy metrics, we now proceed to numerical investigation. To this end, we focus on a minimal yet representative collective configuration: a three-qubit QB system (i.e., $n = 4$ in our model). This setup allows us to explicitly probe the dynamics of rapid charging and energy dissipation regulation across various parameter regimes. In the following section, we will numerically simulate the time evolution of the internal energy $E(t)$ and ergotropy $\mathcal{E}(t)$, analyzing the impact of parameters such as the tunneling strength T_{e}, spectral cutoff ω_0, driving amplitude V, and other key system and environmental controls.

We now specify the Hamiltonian for the three-qubit QB system under study ($n = 4$), which is constructed according to the collective scheme in Fig. 1(b):

$$\hat{H}_{\mathrm{S}} = \begin{bmatrix} \varepsilon_1 & \Omega_{12}(t) & \Omega_{13}(t) & \Omega_{14}(t) \\ \Omega_{21}(t) & \varepsilon_2 & T_{\mathrm{e}} & 0 \\ \Omega_{31}(t) & T_{\mathrm{e}} & \varepsilon_3 & T_{\mathrm{e}} \\ \Omega_{41}(t) & 0 & T_{\mathrm{e}} & \varepsilon_4 \end{bmatrix}. \tag{11}$$

In Eq. (11), the charging functions in the Hamiltonian are defined as

$$\Omega_{12}(t) = \Omega_{21}(t) = V\sin(\Omega t/\tau), \tag{12}$$

$$\Omega_{13}(t) = \Omega_{31}(t) = V[1-\cos(\Omega t/\tau)], \quad (13)$$

$$\Omega_{14}(t) = \Omega_{41}(t) = V\sin(\Omega t/\tau), \quad (14)$$

where V is the amplitude of the charging function, Ω is an integer, and τ is the maximum charging time. $\varepsilon_2 = \varepsilon_3 = \varepsilon_4 = 0.25$ eV, $\varepsilon_1 = 0.25$ eV $+ \Delta E$, and ΔE represents the energy gap. T_e is the tunneling amplitude between different individual battery units.

4. Results and discussion

With the model specified, we now present the numerical analysis of energy storage dynamics in the collective three-qubit QB. The system parameters used in our simulations are summarized in Table 1. The subsequent analysis focuses on the dynamical behavior of energy storage, illustrating how the many-body QB achieves fast charging under various control regimes.

Table 1. Parameters for the collective three-qubit QBs.

	Ω	ΔE (eV)	ω (Hz)	$\gamma\times10^{-7}$ (Hz)	ω_0 (Hz)	T_e	T (K)	V (μV)
Fig. 3(a)	\	1.5	0.085	2.6	0.10	0	300	1.5
Fig. 3(b)	1.0π	\	0.085	2.6	0.12	0	300	1.5
Fig. 3(c)	1.0π	2.75	0.085	2.6	0.12	0	300	\
Fig. 3(d)	1.0π	2.75	0.085	2.6	0.12	\	300	1.5
Fig. 4(a)	1.0π	1.5	0.085	2.6	\	0	300	1.5
Fig. 4(b)	1.0π	1.5	\	9.0	0.12	0	300	1.5
Fig. 4(c)	1.0π	1.5	0.085	\	0.03	0	300	1.5
Fig. 4(d)	1.0π	1.5	0.143	9.0	0.08	0	\	1.5

4.1. Dynamics of ergotropy under driving and intrinsic parameter control

The capability of a QB to undergo rapid-stable charging is a crucial metric of its operational performance. In this section, we examine how various system and driving parameters — including the frequency and amplitude of the charging field, the material bandgap, and the inter-battery tunneling strength — modulate the time-dependent evolution of ergotropy. The results are presented in Fig. 3, where each subfigure corresponds to a specific control parameter.

(a) Frequency dependence As shown in Fig. 3(a), increasing the driving frequency Ω significantly accelerates the charging process, reducing the time to reach the ergotropy plateau by up to 40% (200 fs, as Ω increases from 0.7π to 1.2π, the red dashed line evolves into the blue solid line). The marked enhancement in charging efficiency, however, is a direct manifestation of the collective Λ-structure, wherein the shared excited state acts as a common conduit for coherent excitation. The shared excited state acts as a funnel, allowing the global driving field to coherently excite the entire battery array simultaneously.

(b) Amplitude dependence Figure 3(b) illustrates the influence of the driving-field amplitude V on ergotropy dynamics. At small amplitudes (e.g., $V = 0.25$, 0.6 μV), the peak ergotropy scales nearly linearly with V while the time to reach the peak remains almost unchanged. Beyond a critical threshold (e.g., $V = 3.5$ μV), however, this stable charging behavior collapses, and the ergotropy rapidly decays to zero. This abrupt transition signals the breakdown of the linear-response regime and the rotating-wave approximation: the strong drive activates counter-rotating terms, couples the system to off-resonant modes, and opens irreversible dissipation channels. Concurrently, large V induces multi-level transitions and destructive inter-qubit interference, analogous to Landau–Zener-type nonadiabatic processes.[35] These results highlight the existence of an optimal driving regime for efficient energy storage and point to future directions for controlling drive-induced dissipation in many-body quantum batteries.

(c) Bandgap effect Figure 3(c) shows that the material bandgap ΔE primarily dictates the energy capacity, not the charging rate. We observe an inverse relationship between ΔE and the peak ergotropy — a larger gap diminishes the maximum extractable work. This underscores a fundamental design trade-off: while a larger ΔE offers superior protection against thermal noise, it necessitates higher-energy photons for excitation, which are less efficiently utilized in unitary work-extraction cycles. Our collective model centralizes this trade-off through the single excited state, providing a clear design rule: optimal QB materials should exhibit moderate bandgaps to balance energy density and operational stability.

(d) Tunneling-induced dissipation The interplay of tunneling strength T_e, illustrated in Fig. 3(d), reveals a dynamic phase transition unique to interacting many-body QBs. At weak T_e ($T_e = 0.03$, 0.04), coherent tunneling sustains long-lived ergotropy oscillations, a signature of delocalized excitations across the ground-state manifold. As T_e increases ($T_e = 0.05, 0.06, 0.07, 0.08$), a critical point is crossed where the system abruptly enters an overdamped regime. This is not simple decoherence; it is the tunneling-induced opening of new dissipation channels that disrupt the collective dark states responsible for energy retention. This sharp transition provides a tunable switch between coherent memory-like and rapid energy-dissipation regimes, a feature absent in non-interacting battery designs.[36]

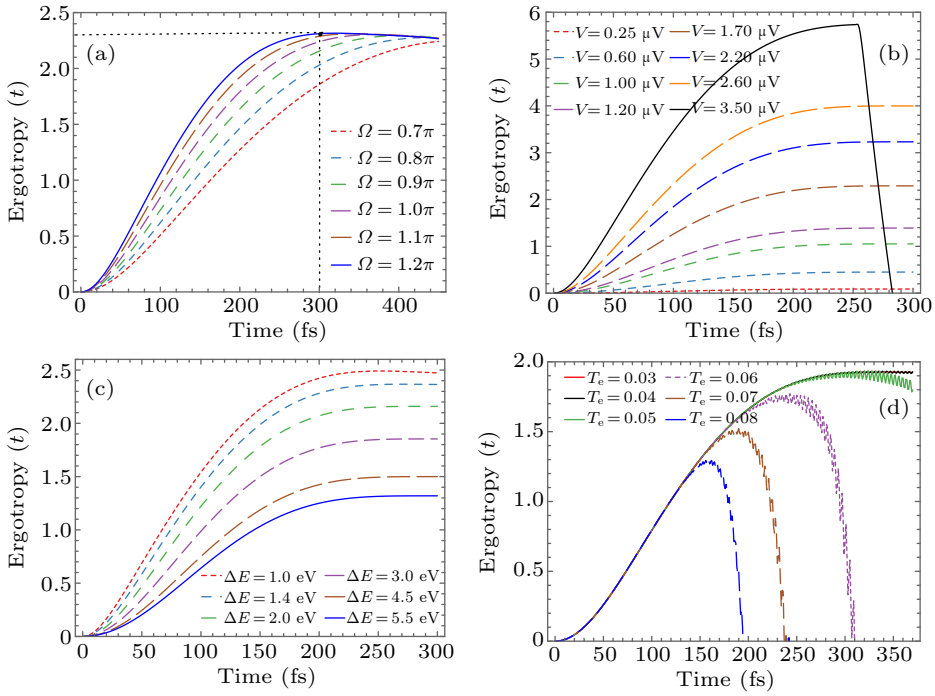

Fig. 3. Time evolution of ergotropy in the collective three-qubit QB model under different control parameters: (a) frequency Ω of the charging field; (b) amplitude V of the charging field; (c) bandgap ΔE of the QB material; (d) inter-QB tunneling strength T_e.

Further long-term simulations (> 300 fs) reveal that the tunneling strength T_e governs a timescale-dependent stability. While ergotropy eventually decays for $T_e \geq 0.05$, there exists a stark contrast in the onset time of collapse. At weak T_e, the battery exhibits a robust quasi-stable plateau, whereas increasing T_e beyond a critical sensitivity point triggers an almost instantaneous energy washout. This suggests that T_e acts as a kinetic switch that controls the activation energy required to escape the coherent-protected manifold into irreversible dissipation channels.

The above analyses collectively reveal a key insight: optimal energy storage requires balancing driving-field strength, material characteristics, and inter-unit coherence. Both overdriving and over-coupling can lead to destructive quantum interference and dissipative losses. Hence, engineering QBs involves not only selecting suitable parameters but also understanding their interplay under the framework of non-Markovian quantum thermodynamics. These findings offer design principles for the development of robust and scalable QB platforms. Having established the role of intrinsic parameters, we now discuss the interplay of collective and environmental effects in shaping the overall QB performance.

The observed collapse in ergotropy during the charging phase is a signature of the system entering the passive state manifold. While the driving field pumps energy into the battery, the irreversible dissipation channels — modeled here via the Redfield-type master equation — simultaneously degrade quantum coherences and reorder energy level populations. According to the passivity theorem, ergotropy vanishes when the state becomes diagonal and energy-ordered, regardless of the total internal energy. The rapid decay in the strong-coupling regime indicates that environmental dissipation effectively "outruns" the coherent charging process, trapping the battery in a zero-extractable-work configuration.

4.2. Dynamics of ergotropy under environmental parameters

Having established the influence of intrinsic system parameters on ergotropy, we now turn to the role of environmental factors — cutoff frequency ω_0, coupling strength γ, spectral profile $J(\omega_k)$, and temperature T — in shaping the charging dynamics, as summarized in Fig. 4.

(a) Cutoff frequency ω_0 and non-Markovian memory The cutoff frequency ω_0, which is inversely related to the environment's correlation time, strongly influences ergotropy stability. As shown in Fig. 4(a), a larger ω_0 (shorter memory) suppresses oscillatory behavior and stabilizes the ergotropy plateau. This stabilization arises because a broadband environment rapidly dephases non-energy-storing coherences, steering the system toward a steady state. These results highlight the potential of engineering the environmental memory timescale as a viable strategy for enhancing QB stability, albeit at a slight cost to peak ergotropy.

(b) Spectral control of decoherence vs. dissipation Figure 4(b), together with the spectral dependence of the Redfield tensor in Fig. 2, reveals a key property of structured non-Markovian environments: the decoupling of pure dephasing from energy relaxation. While a larger ω can suppress the dissipative part of the Redfield tensor (Fig. 2), it simultaneously enhances dephasing through a broader spectrum of vir-

tual modes, leading to the smoother ergotropy profiles shown in Fig. 4(b). This suggests that in strongly coupled regimes, dephasing can stabilize the battery by suppressing parasitic coherences without significant energy loss — a level of control beyond Markovian approximations.

(c) System–environment coupling strength γ As expected, Fig. 4(c) confirms that strong system–environment coupling (large γ) degrades ergotropy by accelerating energy leakage and decoherence. This underscores the challenge of maintaining collective advantages under strong noise. Nevertheless, our model provides a quantitative tool to identify the coupling thresholds at which such advantages erode, paving the way for future studies on protected states in the deep strong-coupling regime.

(d) Environmental temperature T Finally, the temperature dependence in Fig. 4(d) underscores the vulnerability of quantum-enhanced performance to thermal noise. The ergotropy exhibits a sharp decline for $T \geq 100$ K in this Λ-system. This provides a clear operational temperature ceiling for observing the collective benefits predicted by our model, guiding experimental implementations toward cryogenic conditions.

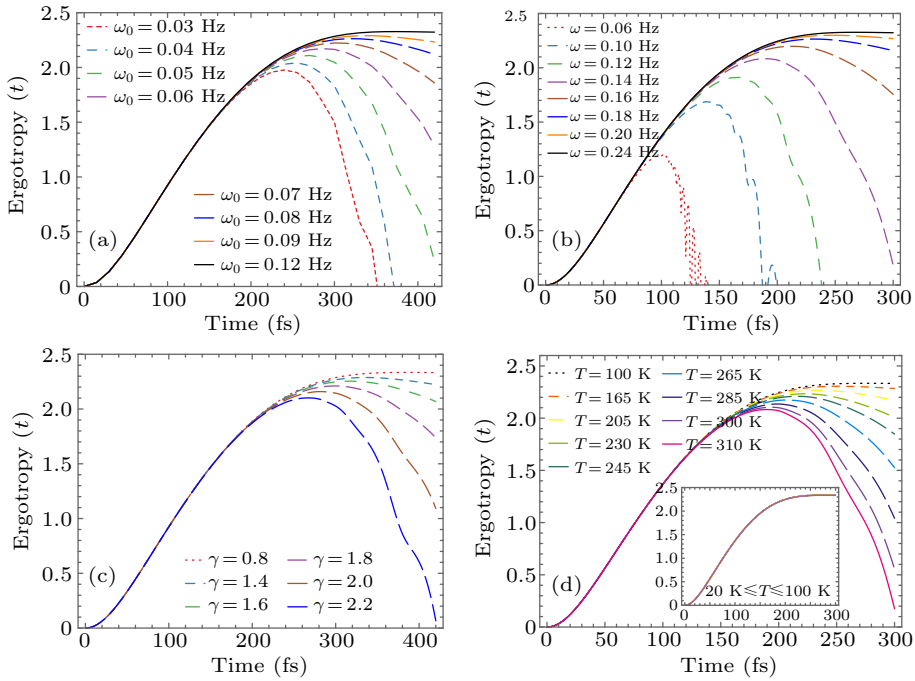

Fig. 4. Ergotropy dynamics under different environmental parameters: (a) cutoff frequency ω_0, (b) spectral profile influence via Redfield tensor, (c) coupling strength γ, and (d) environmental temperature T.

The results in Fig. 4 collectively indicate that environmental factors exert a dual-edged influence on QB performance. While certain environmental modes (e.g., broad ω_0) can help stabilize the output, excessive system–environment interaction (γ) and thermal agitation (high T) are detrimental to energy retention. These insights suggest that optimal ergotropy retrieval in many-body QBs necessitates a fine balance: designing environments that are spectrally rich yet weakly coupled and thermally isolated.

The above findings underscore the dual role of the environment in QB operation. On one hand, an appropriately structured environment, e.g., a broad but weakly coupled spectrum, can promote steady energy output by selectively damping non-useful dynamics. On the other hand, excessive coupling strength or thermal noise can rapidly suppress ergotropy. The insight that ω_0 and T play opposite roles on different time scales offers design flexibility. Specifically, materials with tunable spectral responses or system–bath decoupling techniques can be leveraged to optimize energy storage while preserving ergotropy.

5. Collective charging: mechanisms and realizations

To further elucidate the origin of the collective charging advantage, we analyze the underlying mechanisms distinguishing collective from parallel protocols and discuss feasible experimental platforms where such effects could be observed and verified.

5.1. Origin of collective charging advantage

A central question arises as to whether the rapid and stable charging observed in this work originates primarily from the collective Λ-structure of the QB or from the non-Markovian character of its environment. It should be emphasized that this study does not include numerical simulations of a parallel-charging benchmark; hence, no quantitative superiority of the collective protocol is claimed.

Instead, our analysis focuses on the physical mechanisms through which collective architectures can yield enhanced charging behavior. (i) The shared excited state inherent to the Λ-configuration enables coherent population funneling under a global drive, synchronizing energy transfer across all battery units — a feature absent in parallel systems with independent excitations. (ii) Collective coherent superpositions, including dark states, effectively decouple from dominant dissipative channels, thereby suppressing energy leakage and enhancing energy retention. (iii) The finite memory of the non-Markovian environment induces transient backflow of energy and correlations, modulating coherent dynamics and contributing to charging stability.

Collectively, these mechanisms form a qualitative foundation for understanding potential advantages of collective charging within suitable parameter regimes. A rigorous, quantitative comparison with parallel charging — under matched system parameters or an analytic baseline — remains an important subject for future investigation.

5.2. Possible experimental realization

To examine the physical foundation and experimental feasibility of the proposed collective Λ-type QB, we outline below several realistic implementation strategies based on state-of-the-art platforms.

A promising route involves semiconductor quantum dot arrays, where discrete energy levels can be engineered and tuned via external gate voltages or strain fields. In coupled quantum dots, exciton states may serve as the shared excited level, while two spatially localized ground states form the lower branches of each Λ system.[37,38] Coherent tunneling or dipole–dipole coupling between dots enables population transfer and collective excitation dynamics consistent with our model.

Rydberg atomic ensembles constitute another viable platform. Here, individual atoms possess long-lived ground states and couple collectively to a common highly excited Rydberg state through the dipole blockade mechanism, forming an effective Λ configuration with strong interatomic correlations.[39,40] Recent experiments have demonstrated coherent excitation exchange and energy transport in such systems, providing a suitable setting to probe collective ergotropy effects.[41,42]

The essential requirements of our model — (i) tunable energy gaps across subsystems, (ii) controllable tunneling or coupling strengths, and (iii) a common excited state shared by all units — can be satisfied in both of these architectures, enabling experimental access to the ergotropy dynamics and coherent charging behaviors predicted in our simulations.

Furthermore, superconducting circuit QED systems can emulate effective Λ configurations using transmon qubits coupled to a shared resonator mode, which acts as the common excited level.[43,44] These platforms offer high control fidelity and programmable interactions, and have already been employed in experimental explorations of QB concepts.[21]

In summary, the proposed collective Λ-type QB model is not only theoretically well-founded but also experimentally realizable across multiple architectures — including quantum dots, Rydberg atoms, and superconducting circuits — each offering a feasible pathway to investigate collective charging dynamics and quantum thermodynamic performance.

6. Conclusion

In conclusion, we have proposed a strongly coupled many-body QB model that enables rapid and stable collective charging while effectively suppressing discharge reversals. This model incorporates a non-perturbative treatment of system–environment interactions and allows us to quantitatively analyze the dynamics of ergotropy under various driving and environmental parameters. Our findings demonstrate that enhancing the driving frequency (Ω) and tunneling strength (T_e) can significantly accelerate and stabilize energy storage. In contrast, strong bandgap detuning (ΔE), excessive driving amplitude (V), and increased environmental coupling (γ) may induce non-adiabatic transitions or dissipative effects that degrade performance. Importantly, our results reveal charging dynamics that deviate from classical macroscopic batteries, highlighting intrinsic quantum many-body features that emerge under strong coupling. These effects are concretely characterized through ergotropy profiles and coherence-dependent evolution timescales. Furthermore, our identification of parameters that regulate or suppress energy reversal provides valuable guidance for experimental realization.

Looking ahead, this work suggests promising directions for employing advanced non-perturbative methods, such as tensor-network techniques or HEOM approaches, and motivates future efforts to implement and test these findings in solid-state, photonic, or superconducting platforms. Combined with the proposed experimental schemes, our model may assist the design of programmable QB schemes in experimentally accessible settings.

Appendix A: Microscopic derivation of the redfield-type master equation

To clarify the microscopic foundation of the Redfield-type master equation used in Eq. (6), we briefly outline its derivation starting from the total Hamiltonian defined in Eqs. (1)–(4). We emphasize that the dissipative dynamics employed in this work is not introduced phenomenologically, but follows from a standard second-order perturbative treatment of the system–environment interaction.

The total Hamiltonian reads

$$\hat{H} = \hat{H}_{\rm S} + \hat{H}_{\rm E} + \hat{H}_{\rm int}, \tag{A1}$$

where the interaction Hamiltonian is given by

$$\hat{H}_{\rm int} = \sum_i \hat{A}_{\rm S}^{(i)} \otimes \hat{B}_{\rm E}^{(i)}, \tag{A2}$$

with system operators $\hat{A}_{\rm S}^{(i)} = |g_i\rangle\langle g_i|$ and bath operators $\hat{B}_{\rm E}^{(i)} = \sum_k g_k^{(i)}(\hat{a}_k + \hat{a}_k^\dagger)$, as specified in Eq. (4).

In the interaction picture, the evolution of the reduced density matrix $\rho_{\rm S}(t)$ is obtained by performing a second-order expansion in $\hat{H}_{\rm int}$ under the Born approximation, assuming the environment remains in thermal equilibrium. This leads to the standard Redfield equation

$$\frac{{\rm d}\hat{\rho}_{\rm S}(t)}{{\rm d}t} = -\int_0^\infty {\rm d}\tau\, {\rm Tr}_{\rm E}\left[\hat{H}_{\rm int}(t), \left[\hat{H}_{\rm int}(t-\tau), \hat{\rho}_{\rm S}(t)\otimes\hat{\rho}_{\rm E}\right]\right], \tag{A3}$$

where $\rho_{\rm E}$ denotes the thermal state of the bosonic bath.

Expressed in the energy eigenbasis of $\hat{H}_{\rm S}$, this equation gives rise to the Redfield tensor structure[26] appearing in Eq. (5), with transition rates determined by the bath correlation functions and, equivalently, by the environmental spectral density $J(\omega)$. In this work, we adopt a Debye-type spectral density, which introduces a finite bath correlation time and enables the incorporation of non-Markovian memory effects in a controlled manner.

Therefore, the Redfield-type master equation employed here follows directly from the microscopic Hamiltonian of Eqs. (1)–(4). The resulting dissipative coefficients explicitly encode both the system structure of the collective Λ-type quantum battery and the spectral properties of the environment, providing a physically consistent framework for analyzing ergotropy dynamics beyond purely Markovian approximations.

Appendix B: Entropy production rate and thermodynamic consistency

To verify the consistency of the proposed charging dynamics with the second law of thermodynamics, we analyze the entropy production rate associated with the reduced system dynamics. For an open quantum system governed by a Redfield-type master equation, the entropy production rate[45,46] can be defined in the Spohn form as

$$\dot{\Sigma}(t) = -{\rm Tr}\left[\dot{\hat{\rho}}(t)\left(\ln\hat{\rho}(t) - \ln\hat{\rho}_{\rm G}(t)\right)\right], \tag{B1}$$

where $\rho(t)$ is the instantaneous reduced density matrix and $\rho_{\rm G}$ denotes the instantaneous Gibbs reference state of the dynamics

$$\hat{\rho}_{\rm G}(t) = \frac{{\rm e}^{-\beta\hat{H}_{\rm S}(t)}}{{\rm Tr}\left[{\rm e}^{-\beta\hat{H}_{\rm S}(t)}\right]}$$

with $\beta = 1/(k_{\rm B}T)$. This definition remains applicable beyond the strictly Markovian regime and provides a sufficient criterion for the validity of the second law.

We numerically evaluate Eq. (B1) for different values of the key control parameters, including the frequency Ω of the charging field, the amplitude V of the charging field, the bandgap ΔE of the QB material, and the inter-QB tunneling strength $T_{\rm e}$ in Fig. B1.

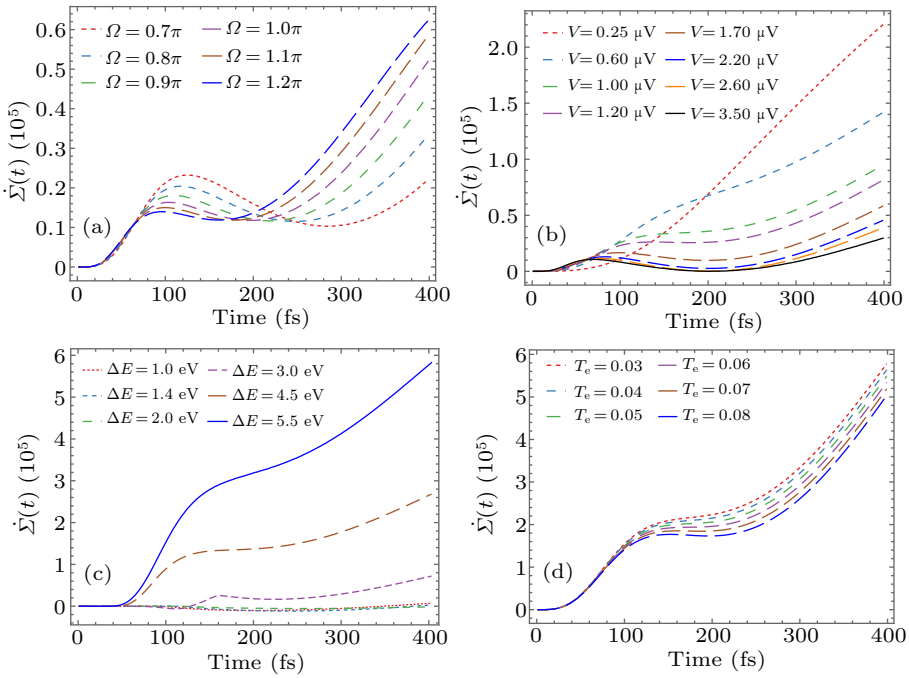

Fig. B1. Time evolution of the entropy production rate in the collective three-qubit QB model under different control parameters: (a) frequency Ω of the charging field; (b) amplitude V of the charging field; (c) bandgap ΔE of the QB material; (d) inter-QB tunneling strength $T_{\rm e}$. Other parameters are the same as those in Fig. 3.

The numerical results show that $\dot{\Sigma}(t)$ remains non-negative over the entire evolution for all parameter sets considered. This positivity is consistent with Spohn's inequality for Markovian generators and maintains its validity within the moderate-coupling regime explored in this work. Such results rigorously confirm that the observed collective charging dynamics — characterized by enhanced charging power and suppressed energy leakage — are fully compatible with the second law of thermodynamics. Furthermore, these thermodynamic foundations provide a self-consistent framework to interpret the stability–dissipation trade-off, ensuring that the performance gains of the quantum battery are physically grounded.

Data availability statement

All data included in this manuscript are available upon reasonable request by contacting the corresponding author.

Acknowledgment

We gratefully acknowledge support of the National Natural Science Foundation of China (Grant Nos. 62065009 and 61565008).

References

[1] Alicki R and Fannes M 2012 *Phys. Rev. E* **87** 042123
[2] Andolina G M, Keck M, Mari A, Campisi M, Giovannetti V and Polini M 2018 *Phys. Rev. Lett.* **122** 047702
[3] Xu F, Ma X F, Zhang Q, Lo H K and Pan J W 2020 *Rev. Mod. Phys.* **92** 025002
[4] Rossini D, Andolina G M, Rosa D, Carrega M and Polini M 2020 *Phys. Rev. Lett.* **125** 236402
[5] Santos A C 2021 *Phys. Rev. E* **103** 042118
[6] Rossini D, Andolina G M, Rosa D, Carrega M and Polini M 2020 *Phys. Rev. Lett.* **125** 236402
[7] Gyhm J, Safranek D and Rosa D 2021 *Phys. Rev. Lett.* **128** 140501
[8] Campaioli F, Pollock F A and Vinjanampathy S 2018 *Quantum batteries* (New York: Springer International Publishing)
[9] Farina D, Andolina G M, Mari A, Polini M and Giovannetti V 2019 *Phys. Rev. B* **99** 035421
[10] Rossini D, Andolina G M and Polini M 2019 *Phys. Rev. B* **100** 115142
[11] Julia-Farre S, Salamon T, Riera A, Bera M N and Lewenstein M 2020 *Phys. Rev. Res.* **2** 023113
[12] Tirone S, Salvia R, Chessa S and Giovannetti V 2023 *Phys. Rev. Lett.* **131** 060402
[13] Song W, Liu H, Zhou B, Yang W and An J 2024 *Phys. Rev. Lett.* **132** 090401
[14] Seah S, Perarnau-Llobet M, Haack G, Brunner N and Nimmrichter S 2021 *Phys. Rev. Lett.* **127** 100601
[15] Cakmak B 2020 *Phys. Rev. E* **102** 042111
[16] Julia-Farre S, Salamon T, Riera A, Bera M N and Lewenstein M 2018 *Phys. Rev. Research* **2** 023113
[17] Le T P, Levinsen J, Modi K, Parish M M and Pollock F A 2017 *Phys. Rev. A* **97** 022106
[18] Zhang Y, Yang T, Fu L and Wang X 2018 *Phys. Rev. E* **99** 052106
[19] Andolina G M, Pellegrino F M D, Giovannetti V, MacDonald A H and Polini M 2019 *Phys. Rev. B* **100** 121109
[20] Kamin F H, Tabesh F, Salimi S and Santos A C 2020 *Phys. Rev. E* **102** 052109
[21] Dou F Q and Yang F M 2023 *Phys. Rev. A* **107** 023725
[22] Shi H L, *et al*. 2022 *Phys. Rev. Lett.* **129** 130602
[23] Mondal S and Bhattacharjee S 2021 *Phys. Rev. E* **105** 044125
[24] Fleischhauer M, Imamoglu A and Marangos J P 2005 *Rev. Mod. Phys.* **77** 633
[25] Kubo R 1966 *Rep. Prog. Phys.* **29** 255
[26] Redfield A G 1965 *Advances in Magnetic and Optical Resonance* Vol. 1 (Academic Press) pp. 1–32
[27] Crowder E, Lampert L, Manchanda G, Shoffeitt B, Gadamsetty S, Pei Y, Chaudhary S and Davidovic D 2024 *Phys. Rev. A* **109** 052205
[28] Becker T, Schnell A and Thingna J 2022 *Phys. Rev. Lett.* **129** 200403
[29] Zhao P L, *et al*. 2016 *Phys. Rev. E* **94** 022126
[30] Kubo R 1966 *Rep. Prog. Phys.* **29** 255
[31] Leggett A J, Chakravarty S, Dorsey A T, Fisher M P A, Garg A and Zwerger W 1987 *Rev. Mod. Phys.* **59** 1
[32] Drude P 1900 *Ann. Phys.* **306** 566
[33] Zhu W, Zhao X and Tang Y 1996 *J. Chem. Phys.* **104** 2275
[34] Allahverdyan A E, Balian R and Nieuwenhuizen T M 2004 *Europhys. Lett.* **67** 565
[35] Altland A, Gurarie V, Kriecherbauer T and Polkovnikov A 2008 *J. Phys. A* **41** 195301
[36] Zhong S Q, Zhao S C and Zhu S N 2021 *Results Phys.* **24** 104094
[37] Krenner H J, *et al*. 2005 *Phys. Rev. Lett.* **94** 057402
[38] Stinaff E A, *et al*. 2006 *Science* **311** 636
[39] Saffman M, Walker T G and Molmer K 2010 *Rev. Mod. Phys.* **82** 2313
[40] Comparat D and Pillet P 2010 *J. Opt. Soc. Am. B* **27** A208
[41] Bernien H, *et al*. 2017 *Nature* **551** 579
[42] Omran A, *et al*. 2019 *Science* **365** 570
[43] Koch J, *et al*. 2007 *Phys. Rev. A* **76** 042319
[44] Blais A, *et al*. 2021 *Rev. Mod. Phys.* **93** 025005
[45] Spohn H 1978 *J. Math. Phys.* **19** 1227
[46] Breuer H P and Petruccione F 2002 *The Theory of Open Quantum Systems* (Oxford: Oxford University Press)